PHYSICAL REVIEW B VOLUME 38, NUMBER 7 1 SEPTEMBER 1988

Early stages of spinodal decomposition for the Cahn-Hilliard-Cook model of phase separation

K. R. Elder, T. M. Rogers, and Rashmi C. Desai
Department of Physics, University of Toronto, Toronto, Ontario, Canada M5S 1A7
(Received 1 February 1988)

A computer simulation using discretized space and time is employed to examine the early stages of phase separation as described by the Cahn-Hilliard-Cook equation (CHCE). The relative simplicity of this simulation provides a direct test of various mathematical treatments of the nonlinear term in the CHCE. In particular, the numerical results are used to ascertain the validity of the approximations inherent in the perturbative expansions of Grant, San Miguel, Vinals, and Gunton, and of Langer, Bar-on, and Miller. The time of validity of all approximations is shown to be logarithmically related to the strength of the thermal fluctuations. In addition, the effect of the initial state on the dynamical evolution of the order parameter is examined.

I. INTRODUCTION

When a system is quenched from a single-phase equilibrium state to an unstable one, spatial inhomogeneities in the order parameter grow as the system evolves to its final two-phase equilibrium state. The widespread appearance of this phenomenon (usually referred to as spinodal decomposition) has prompted many theoretical, numerical, and experimental undertakings.[1-34] Experimental and numerical works have contributed substantially to the qualitative understanding of this complex process while theoretical progress has been hindered by the inherent nonlinear nature of phase separation. How these nonlinearities affect the order-parameter morphology for a simple dynamical model of phase separation with a conserved order parameter [i.e., the Cahn-Hilliard-Cook equation (CHCE)] is examined through numerical simulation.

The difficulty in solving this intricate problem is that the appropriate dynamical equations do not fall within the small subset of solvable nonlinear equations. A standard linearization of the equations of motion was first discussed by Cahn, Hilliard, and Cook.[2-5] Although correctly identifying the initial instability to thermal fluctuations, their theory fails to account for the formation of domain walls and subsequent cluster growth. Some experiments[32,34] and computer simulations[17,20] have shown this theory to be adequate for the very early stages of phase separation while others[15,28,33] exhibit no evidence of the linear predictions. Recent work[11,13,20] indicates that the time of validity of this theory is related to the effective range of interaction. A quantitative assessment of this linear scheme is provided in this paper.

More advanced theories have been proposed in recent years to deal with the nonlinear term in the CHCE. Langer *et al.*[6,7] developed two related schemes whereby physical assumptions were made to simplify the CHCE. These theories mark a considerable improvement over the linear theory but cannot predict the observed late stage behavior. Their major shortcoming is that the direct coupling of Fourier modes implicit in the CHCE is replaced with a "mean-field" type of coupling. A consequence of this mean-field coupling is the inability to describe the transition from spinodal decomposition to nucleation.[10] Approximations similar to those of Langer *et al.*[6,7] will be compared with the numerical simulation.

In 1985 Grant *et al.*[12] developed a systematic expansion in the strength of the nonlinearity which is related to the inverse of the range of interaction. The first term in the expansion reproduces the linear theory of Cahn *et al.*[2-5] Each successive term grows exponentially in time and progressively includes more of the direct coupling needed to form sharp interfaces. Every term in the expansion must be included to account for the long time behavior. The improvement the first-order correction term provides over the linear solution is examined.

In this paper the early stages of phase separation for a conserved order parameter are studied numerically using a discrete version of the CHCE. In addition, the approximations contained in the early time theories are used to construct analogous theories for the discrete system. This formulation is used so that comparisons of the numerical results and the *discrete* theories are decoupled from differences between the continuous and discrete systems. The regime of validity of the theories can then be obtained by a direct comparison with the numerical solution. A nice feature of these comparisons is that only one question is asked, i.e., are these theories a good approximation to the discrete CHCE? In contrast, when these theories are compared with other simulations (e.g., Monte Carlo and molecular dynamics) and experiments this question cannot be unambiguously answered since the CHCE may not exactly describe the system under consideration.

Another interesting aspect of this problem is the effect the initial state has on the dynamical evolution of the order-parameter morphology. In this work the initial (i.e., prequench) configurations were constructed to be consistent with an Ornstein-Zernike structure factor. Unlike laboratory experiments, a numerical simulation allows the precise form and magnitude of this state to be carefully controlled and enables a systematic analysis of the initial state.

The remainder of this paper consists of three sections.

Section II describes the early time theories and emphasizes the deficiencies of these approaches. Results of the numerical simulation are then presented to illustrate the phenomena and examine the validity of the early time predictions. A discussion of these results and a summary of the findings follow.

II. EARLY-TIME THEORIES

The prototype model of phase separation considered in this paper was developed by Cahn, Hilliard, and Cook.[2-5] Although initially derived for binary alloys (with a conserved order parameter), it is also appropriate in other situations such as in polymer mixtures and some magnetic systems. In this formulation the time derivative of the fluctuations in the order parameter (ϕ) is related to the coarse-grained free energy (F) in the following manner,

$$\frac{\partial\phi(\mathbf{r},t)}{\partial t}=M\nabla^2\frac{\delta F}{\delta\phi}+\zeta(\mathbf{r},t)\ , \tag{2.1}$$

where

$$F\{\phi\}=\int d^d r\left[f(\phi)+\frac{\kappa}{2}(\nabla\phi)^2\right]\ , \tag{2.2}$$

$$\langle\zeta(\mathbf{r},t)\zeta(\mathbf{r}',t')\rangle=-2k_B TM\nabla^2\delta(\mathbf{r}-\mathbf{r}')\delta(t-t')\ . \tag{2.3}$$

In Eqs. (2.1), (2.2), and (2.3), M is the mobility, k_B is Boltzmann's constant, T is the temperature, and κ is a positive phenomenological constant that is related to the range of interaction. $f(\phi)$ is the free-energy density of the bulk. In single-phase equilibrium, $f(\phi)$ has a stable single-well structure and can be approximated as

$$f_{\rm eq}(\phi)=\frac{r_{\rm eq}}{2}\phi^2\ . \tag{2.4}$$

In the two-phase region, $f(\phi)$ has a double-well structure and in this model has the form

$$f_{\rm ne}(\phi)=-\frac{r_{\rm ne}}{2}\phi^2+\frac{u_{\rm ne}}{4}\phi^4\ . \tag{2.5}$$

$r_{\rm eq}$, $r_{\rm ne}$, and $u_{\rm ne}$ are also positive phenomenological constants. Following the work of Grant *et al.*,[12] it is convenient to convert Eqs. (2.1), (2.2), (2.3), and (2.5) to a dimensionless form by making the following transformation of variables:

$$\mathbf{x}=\left[\frac{r_{\rm ne}}{\kappa_{\rm ne}}\right]^{1/2}\mathbf{r}\ ,$$

$$\tau=\left[\frac{2Mr_{\rm ne}^2}{\kappa_{\rm ne}}\right]t\ ,$$

$$\psi=\left[\frac{u_{\rm ne}}{r_{\rm ne}}\right]^{1/2}\phi\ .$$

It is theoretically convenient to restrict the parameters of the single-phase system in the following manner:

$$\frac{r_{\rm ne}}{\kappa_{\rm ne}}=\frac{r_{\rm eq}}{\kappa_{\rm eq}}\ . \tag{2.6}$$

Equation (2.6) restricts the prequench state to be a function of only one parameter. In this notation the equation of motion in the single phase is

$$\frac{\partial\psi(\mathbf{x},\tau)}{\partial\tau}=\frac{\nabla^2}{2}[\psi(\mathbf{x},\tau)-\nabla^2\psi(\mathbf{x},\tau)]+\sqrt{\epsilon_I}\mu(\mathbf{x},\tau)\ , \tag{2.7}$$

where

$$\langle\mu(\mathbf{x},\tau)\mu(\mathbf{x}',\tau')\rangle=-\nabla^2\delta(\mathbf{x}-\mathbf{x}')\delta(\tau-\tau')$$

and

$$\epsilon_I=\epsilon_N\left[\frac{r_{\rm ne}T_{\rm eq}}{r_{\rm eq}T_{\rm ne}}\right]\ .$$

The stationary or equilibrium solution of Eq. (2.7) for the structure factor $S(k,\infty)$ has the usual Ornstein-Zernike form:

$$S(k,\infty)=\frac{\epsilon_I}{k^2+1}\ , \tag{2.8}$$

where

$$S(k,\tau)=\langle\psi_{\mathbf{k}}\psi_{\mathbf{k}}^*\rangle\ .$$

In the two-phase region the dimensionless equation of motion for ψ is

$$\frac{\partial\psi(\mathbf{x},\tau)}{\partial\tau}=-\frac{\nabla^2}{2}[\psi(\mathbf{x},\tau)-\psi^3(\mathbf{x},\tau)+\nabla^2\psi(\mathbf{x},\tau)]+\sqrt{\epsilon_N}\mu(\mathbf{x},\tau)\ , \tag{2.9}$$

where

$$\epsilon_N=\frac{k_B T_{\rm ne}u_{\rm ne}}{r_{\rm ne}^2}\left[\frac{r_{\rm ne}}{\kappa_{\rm ne}}\right]^{d/2}\ .$$

Equation (2.8) will be used as the initial $S(k,\tau=0)$ for both the numerical and theoretical work. In this framework the problem contains two dimensionless parameters, ϵ_I and ϵ_N. ϵ_I is related to the strength of the prequench fluctuations and ϵ_N is related to the strength of the thermal fluctuations after the quench. ϵ_N is also proportional to the inverse of the range of interaction. For most of the simulations performed in this work $\epsilon_I=\epsilon_N$. The reason for this will become apparent when studying the linear expansion theory.

The theories considered in this paper will be classified as linear (LT) or nonlinear (NLT) types. LT are based on an expansion in the linear operator as derived by Grant *et al.*[12] In contrast, NLT do not rely on the linear solution but use physical assumptions to simplify the problem. To evaluate the validity of these theories a numerical simulation of Eq. (2.9) was performed.

In the simulation a finite difference scheme (i.e., Euler's method) is employed to account for both the temporal and spatial derivatives as discussed in Refs. 18, 21, 22, 23, 26, and 27. This discretization scheme introduces two dimensionless parameters, the mesh size (Δx) and the time step ($\Delta\tau$). As noted in Ref. 27, these parameters must be chosen carefully to avoid unphysical solutions (e.g., subharmonic bifurcations). To facilitate comparison of theory and simulation it is useful to consider Eq. (2.9) in

discrete Fourier space,

$$\psi_{\mathbf{k}}(n+1)=a(k)\psi_{\mathbf{k}}(n)+\sqrt{\epsilon_N}\mu(\mathbf{k},n) +b(k)\sum_{\mathbf{k}'}\sum_{\mathbf{k}''}\psi_{\mathbf{k}'}(n)\psi_{\mathbf{k}''}(n)\psi_{\mathbf{k}-\mathbf{k}'-\mathbf{k}''}(n) , \tag{2.10}$$

where

$$\Gamma(k)=\frac{2}{\Delta x^2}[\cos(k_x\Delta x)+\cos(k_y\Delta x)-2] ,$$

$$a(k)=1-\Delta\tau\Gamma(k)[1+\Gamma(k)]/2 ,$$

$$b(k)=\frac{\Delta\tau}{2}\Gamma(k) ,$$

and

$$\langle\mu(\mathbf{k},\tau)\mu(\mathbf{k}',\tau')\rangle=-\frac{\Delta\tau}{(\Delta x)^d}\Gamma(k)\delta_{\mathbf{k},-\mathbf{k}}\delta_{\tau,\tau'} .$$

$\psi_{\mathbf{k}}$ is the discrete Fourier transform of ψ, i.e.,

$$\psi_{\mathbf{k}}=\frac{1}{N^2}\sum_{\mathbf{x}}\psi_{\mathbf{x}}e^{i\mathbf{x}\cdot\mathbf{k}} ,$$

where

$$\mathbf{k}=\frac{2\pi}{N\Delta x}(l\hat{\mathbf{x}}+m\hat{\mathbf{y}}) .$$

n is the number of time steps covered in time τ for step size $\Delta\tau$. The indices l and m cover the entire lattice [e.g., $l,m\in(1,N)$] of an $N\times N$ system. The function $\Gamma(k)$ is the Fourier transform of ∇^2. In the continuum limit (i.e., in the limit $\Delta x\to 0$), $\Gamma(k)=-(k_x^2+k_y^2)^{1/2}$. In the following sections it will become apparent that all the theoretical structure factors are in fact functionals of $\Gamma(k)$. Thus when "k" is used it will refer to $\sqrt{-\Gamma(k)}$.

One advantage of using a simple finite difference algorithm is that the discrete analog of the continuous early-time theories[2–7,12] can be easily determined. It should be made clear that the simulations are only compared with the discrete versions of the early-time theories. The following sections describe the discrete formulation of the LT and NLT theories.

A. Linear-type theory

In a manner similar to Ref. 12, a perturbative expansion for Eq. (2.10) can be developed using the linear operator to account for the nonlinearity. For pedogogical reasons it is useful to consider the case $\epsilon_N=0$. In this simplified example the formal solution to Eq. (2.10) is

$$\psi_{\mathbf{k}}(n)=[a(k)+b(k)Q]^n\psi_{\mathbf{k}}(n=0) . \tag{2.11}$$

Q is a nonlinear operator that acts on an arbitrary function ($h_{\mathbf{k}}$) of k in the following manner:

$$Qh_{\mathbf{k}}=\sum_{\mathbf{k}'}\sum_{\mathbf{k}''}h_{\mathbf{k}'}h_{\mathbf{k}''}h_{\mathbf{k}-\mathbf{k}'-\mathbf{k}''} .$$

An expansion in terms of $\psi_{\mathbf{k}}(0)$ and $a(k)^n$ can be obtained by using the identity

$$[a(k)+b(k)Q]^n\psi_{\mathbf{k}}(0)=a(k)^n\psi_{\mathbf{k}}(0)+a(k)^n\sum_{m=1}^{n}a(k)^{-m}b(k)Q[a(k)+bQ]^{m-1}\psi_{\mathbf{k}}(0) . \tag{2.12}$$

Equation (2.12) can be proved by induction. The first term [i.e., $a^n\psi_{\mathbf{k}}(0)$] in the series is not influenced by any other $\psi_{\mathbf{k}'}$ ($\mathbf{k}'\neq\mathbf{k}$) and in this sense does not include any mode coupling. The next term in the expansion is

$$a(k)^n b(k)\sum_{m=1}^{n}a(k)^{-m}\sum_{\mathbf{k}'}\sum_{\mathbf{k}''}[a(k-k'-k'')a(k')a(k'')]^{m-1}\psi_{\mathbf{k}'}(0)\psi_{\mathbf{k}''}(0)\psi_{\mathbf{k}-\mathbf{k}'-\mathbf{k}''}(0) . \tag{2.13}$$

The summation over m can be easily performed by noting that Eq. (2.13) is a geometric series. The above term has the effect of coupling in more of the Fourier modes. For example, if $\psi_{\mathbf{k}}(0)\sim\delta_{k,k_0}$, then Eq. (2.13) gives a nonzero contribution to $\psi_{\mathbf{k}_0}$ and $\psi_{3\mathbf{k}_0}$. The next term in the expansion would influence $\psi_{\mathbf{k}_0}$, $\psi_{3\mathbf{k}_0}$, and $\psi_{5\mathbf{k}_0}$, and so on. Thus each term in the expansion has the effect of stimulating higher order Fourier modes.

An interesting feature of this expansion is that it possesses the structure

$$\psi(n)\sim a^n\psi(0)+a^{3n}\psi^3(0)+a^{5n}\psi^5(0)+\cdots .$$

The expansion parameter is thus $a^n\psi_{\mathbf{k}}(0)$, where a^n is equivalent to $e^{k^2(1-k^2)\tau/2}$ in continuous space. If the initial condition is of the form described in Eq. (2.8) [i.e., $\psi_{\mathbf{k}}(0)\sim\sqrt{\epsilon_I}$] then the expansion parameter is of the form $\epsilon_I e^{w\tau}$ in continuous space. For some modes w is positive so that the expansion parameter diverges with time. This is a common result when a linear expansion is performed on a nonlinear equation.[35] The breakdown of the perturbation theory stems from the instabilities in the nonlinear equation. The expansion will only be valid at early times when $\epsilon_I e^{w\tau}$ is small.

When the thermal noise is nonzero (i.e., $\epsilon_N\neq 0$) the situation is more complicated but the above comments still apply. In this case, each term in the expansion will be multiplied by combinations of ϵ_I and ϵ_N. A perturbative expansion in one variable is obtained by setting $\epsilon=\epsilon_I=\epsilon_N$. Under these conditions $S(k,\tau)$ can be realized in terms of a power series expansion in ϵ, i.e.,

$$S(k,\tau)=\epsilon S_1(k,\tau)+\epsilon^2 S_3(k,\tau)+\epsilon^3 S_5(k,\tau)+\cdots . \tag{2.14}$$

(The terms proportional to ϵ to the half-integer power are zero.) The linear solution [i.e., $S_1(k,\tau)$] will be denoted as LT I, the solution to order ϵ^2 as LT II and so on.

When the discrete version of Eq. (2.7) is used to generate the initial state the linear solution is

$$S_1(k,n)=-\Delta\tau\Gamma(k)\left[\epsilon_I\frac{a^{2n}(k)}{1-d^2(k)}+\epsilon_N\frac{1-a^{2n}(k)}{1-a^2(k)}\right], \tag{2.15}$$

where

$$d(k)=1+\Delta\tau\Gamma(k)\{1-\Gamma(k)\}/2 .$$

In the $n=0$ limit, Eq. (2.15) reduces to the discrete version of Eq. (2.8). The first term in Eq. (2.15) is due to the initial state and the second is due to thermal fluctuations. Originally Cahn and Hilliard[2] derived the continuous version of this equation without fluctuations and several years later Cook[4,5] included the term due to fluctuations. Equation (2.15) correctly identifies the initial instability and predicts an exponential growth for wave vectors less than 1. The instability corresponds to the tangential bifurcation[27] arising in a linear stability analysis of Eq. (2.10). Competition between the initial state and thermal fluctuations causes the maximum in $S(k,\tau)$ to move from around 1 to $1/\sqrt{2}$, after which it remains time independent (for $\epsilon_I=\epsilon_N$). The linear predictions for $S(k,\tau)$ clearly disagree with the late-stage power-law growth and coarsening observed in experiments[28–34] and simulations.[15–27]

Recently Binder[11,13] has shown that the time of validity of LT I ($\tau_{\max}$) can be related to the logarithm of ϵ. Specifically the relationship was shown to be $\tau_{\max}\leq -4\ln(3\epsilon)$ (for $\epsilon_I=\epsilon_N=\epsilon$). The logarithmic dependence of $\tau_{\max}$ on ϵ can be understood by realizing that the linear approximation is equivalent to assuming $f(\psi)\simeq-\psi^2/2$ [see Eq. (2.5)]. Thus the linear theory will only be valid if the distribution of ψ's is such that $\psi^2\gg\psi^4/2$. If one assumes this inequality is violated when $\langle\psi^2\rangle$ is approximately equal to some constant (C) then the time of validity ($\tau_{\max}$) of linear theory must be related to C in the following fashion:

$$C\sim\epsilon e^{a\tau_{\max}}$$

(since in this scheme $\langle\psi^2\rangle\sim\epsilon e^{a\tau_{\max}}$ for $\epsilon=\epsilon_I=\epsilon_N$). In an experiment, the initial state may have an ϵ_I is such that the inequality $\psi^2\gg\psi^4/2$ is already violated and hence LT I will never work. For this reason it is not surprising that some experiments agree with LT I while others do not.

The first-order correction term $[S_3(k,\tau)]$ given in Appendix A reduces to the analogous continuum term found in Ref. 12. The complexity of this expression [see Eq. (A1)] illustrates the practical difficulty in evaluating higher-order terms. Unfortunate as this is, the value of this formally exact solution should not be underestimated. For example, it may be possible to sum an infinite class of terms in some limiting cases as was done for the late-stage limit in the nonconserved case.[36] A quantitative assessment of the validity of LT I and LT II will be provided later on in this paper.

B. Nonlinear-type theories

A relatively simple approximation to Eq. (2.10) can be made by assuming the dominant contributions to $\psi_{\mathbf{k}}$ from the double sum,

$$\sum_{\mathbf{k}'}\sum_{\mathbf{k}''}\psi_{\mathbf{k}'}(n)\psi_{\mathbf{k}''}(n)\psi_{\mathbf{k}-\mathbf{k}'-\mathbf{k}''}(n) ,$$

contain at least one $\psi_{\mathbf{k}}(n)$. Mathematically this amounts to keeping only the terms for which $\mathbf{k}'=-\mathbf{k}''$, $\mathbf{k}'=\mathbf{k}$, and $\mathbf{k}''=\mathbf{k}$. The equation of motion (EOM) for $S(k,\tau)$ is then

$$S(k,n+1)=[a(k)+b(k)f(n)]^2S(k,n)+\epsilon_N\Gamma(k) , \tag{2.16}$$

where

$$f(n)=3\langle\psi^2(n)\rangle .$$

Although this approximation does not produce an analytic solution (as the linear type theories do), it does simplify the nonlinearity by decoupling $S(k,\tau)$ from the infinite hierarchy of higher-order correlation functions. This approximation will be denoted as NLT I (Gaussian) and in the continuous limit is identical to the Gaussian approximation discussed in Ref. 6.

One drawback to this scheme is that $S(k,\tau)$ is no longer directly coupled to $\psi_{\mathbf{k}'}$, for $\mathbf{k}'\neq\mathbf{k}$. This direct coupling is replaced by a "mean-field" approximation in which all the other Fourier modes combine to produce an effective coupling coefficient, $3\langle\psi^2\rangle$. In addition, NLT I (Gaussian) predicts a single-peaked, one-point distribution function $[\rho_1(\psi(\mathbf{x}))]$, centered at $\psi=0$ for a critical quench. Since the final distribution is bimodal, NLT I (Gaussian) must break down before clusters are formed.

In 1975, Langer, Bar-on, and Miller[7] (LBM) introduced a more advanced scheme that allowed $\rho_1(\psi(\mathbf{x}))$ to form a bimodal shape. In brief, this theory makes two fundamental approximations, one for the two-point distribution function $[\rho_2(\psi(\mathbf{x}_1),\psi(\mathbf{x}_2))]$ and the other for $\rho_1(\psi(\mathbf{x}))$. The first approximation serves to truncate the infinite hierarchy of coupled EOM's for the correlation functions while the latter truncates the infinite hierarchy of coupled EOM's for the moments (where $\langle\psi^n\rangle$ is the nth moment). The first approximation is obtained by assuming $\rho_2(\psi(\mathbf{x}_1),\psi(\mathbf{x}_2))/\rho_1(\psi(\mathbf{x}_1))\rho_1(\psi(\mathbf{x}_2))$ can be written as a series expansion in $\psi(\mathbf{x}_1)$ and $\psi(\mathbf{x}_2)$. Using the usual normalization conditions[7] for $\rho_1(\psi(\mathbf{x}))$ and $\rho_2(\psi(\mathbf{x}_1),\psi(\mathbf{x}_2))$ to solve for the unknown coefficients in this series one obtains

$$\rho_2(\psi(\mathbf{x}_1,n),\psi(\mathbf{x}_2,n))=\rho_1(\psi(\mathbf{x}_1,n))\rho_1(\psi(\mathbf{x}_2,n))[1+g(|\mathbf{x}_1-\mathbf{x}_2|,n)\psi(\mathbf{x}_1,n)\psi(\mathbf{x}_2,n)] , \tag{2.17}$$

where $g(x,n)$ is the pair correlation function. It is the inverse Fourier transform of $S(k,n)$, i.e.,

$$g(x,n)=\sum_{\mathbf{k}} S(k,n)e^{-i\mathbf{x}\cdot\mathbf{k}} .$$

Equation (2.17) leads directly to the following EOM for $S(k,n)$:

$$S(k,n+1)=[a(k)+b(k)f(n)]^2S(k,n)+\epsilon_N\Gamma(k) +b^2(k)\left[\langle\psi^6(n)\rangle-\frac{\langle\psi^4(n)\rangle^2}{\langle\psi^2(n)\rangle}\right], \quad (2.18)$$

where

$$f(n)=\frac{\langle\psi^4(n)\rangle}{\langle\psi^2(n)\rangle} .$$

Before discussing the moment EOM's it is interesting to note that Eq. (2.18) contains a structure similar to NLT I (Gaussian). Once again, the direct coupling of Fourier components of the order parameter is approximated by a "mean-field" type coupling. This approach has serious implications for the prediction of the late-stage growth law of the average domain size $[R(\tau)]$. The full nonlinear equation is believed[26,27] to predict that $R(\tau)\sim\tau^{1/3}$ while Eq. (2.18) leads to a growth exponent that is much closer to $\frac{1}{4}$.[7,8] Thus equations of the form (2.18) should only be valid in the early stages of phase separation.

In order to obtain an equation of motion for the moments, LBM approximated $\rho_1(\psi(\mathbf{x}))$ as the sum of two Gaussians, i.e.,

$$\rho_1(\psi)=[2\sigma(2\pi)^{1/2}]^{-1}\left[\exp\left[-\frac{(\psi-b)^2}{2\sigma^2}\right] +\exp\left[-\frac{(\psi+b)^2}{2\sigma^2}\right]\right] . \quad (2.19)$$

The time-dependent parameters σ and b are then related to the second and fourth moments. σ describes the width of each peak while b indicates the distance that the peaks are displaced from zero. In the continuous formulation, Eqs. (2.17) and (2.19) are sufficient to close the set of moment EOM's at two.

In discrete time $\langle\psi^4_{n+1}\rangle$ is a function of four-body correlations and thus Eq. (2.19) is not enough to close the set of equations. In this work the one- and two-point correlations are assumed to be much greater than the higher-order correlations. The resulting EOM $\langle\psi^4\rangle$ is given in Appendix B. This theory will be denoted NLT II (LBM) and in the continuous limit the EOM's for $S(k,\tau)$ and $\langle\psi^4\rangle$ are identical to those used by LBM.

A nice critique of these nonlinear schemes can be found in papers by Binder *et al.*[8,9] The major criticism surrounding the NLT theories is that they predict infinite lifetimes of metastable states since mean-field coupling cannot predict the nucleating clusters which initiate phase separation. Although a nucleating cluster is not needed to start phase separation in spinodal decomposition (where the postquench states are unstable), the inability to generate such clusters with well-defined domain walls restricts the validity of the nonlinear theories to the early stages.

III. RESULTS

All simulations were performed on a 30×30 two-dimensional lattice with periodic boundary conditions, Two-hundred and fifty trials were executed for a given run. Each trial started from an equilibrium state created by simulating the discrete analog of Eq. (2.7). Two thousand time steps ($\tau=600$) were run for each equilibrium state to ensure the structure factor was well within statistical error of the exact stationary solution [i.e., Eq. (2.15) with $n=0$]. Only one set of equilibrium states was needed since the equilibrium state scales with ϵ_I. The statistics for these runs was such that the standard deviation for each mode of $S(k,\tau)$ was 3–4 %.

To examine the regime of validity of all theories, several runs were performed for the case $\epsilon=\epsilon_I=\epsilon_N$. Since $\tau_{\max}$ is expected to vary with $\ln(\epsilon)$, six decades of ϵ were examined (see Table I). The effect of the initial condition was studied for the case of $\epsilon_N=10^{-3}$. In these runs ϵ_I was varied from 10^{-4} to 10^{-1} (see Table II).

The circularly averaged structure factor $S(k,\tau)$ was computed in the following manner:

$$S(k,\tau)=\frac{\sum'_{l,m} S(l,m,\tau)}{\sum'_{l,m} 1} . \quad (3.1)$$

Here $\sum'_{l,m}$ is a sum over all l and m such that $\sqrt{-\Gamma(l,m)}=k$, and

$$S(l,m,\tau)=\frac{\sum_t \psi(l,m,\tau)\psi^*(l,m,\tau)}{\sum_t 1} .$$

$\sum_t$ is a sum over all trials for a given run. Asymmetry of $S(l,m,\tau)$ was examined by comparing its value along the diagonals with the average of its vertical and horizontal components (in addition all other directions were examined in a grey-scale plot[24]). For the statistics of this simulation, asymmetry effects were not observed for any of the runs described in Tables I and II, unlike recent Monte Carlo simulations.[24]

To determine the average domain size $R(\tau)$, the pair-correlation function $g(\mathbf{x},\tau)$ was calculated by taking the inverse Fourier transform of $S(l,m,\tau)$. $R(\tau)$ was then

TABLE I. Runs for $\epsilon=\epsilon_I=\epsilon_N$. In each run 250 trials were performed with $\Delta x=1.7$ and $\Delta\tau=0.3$.

Run	ϵ	τ_{final}
A	1×10^{-1}	80
B	3×10^{-2}	33
C	1×10^{-2}	80
D	3×10^{-3}	45
E	1×10^{-3}	180
F	3×10^{-4}	60
G	1×10^{-4}	80
H	3×10^{-5}	72
I	1×10^{-5}	80
J	3×10^{-6}	80
K	1×10^{-6}	80

TABLE II. Runs for $\epsilon_N = 0.001$. In each run 250 trials were performed with $\Delta x = 1.7$ and $\Delta\tau = 0.3$.

Run	ϵ_I	τ_{final}
L	1×10^{-1}	80
M	1×10^{-2}	80
N	1×10^{-4}	80

defined as the first zero of the spherically averaged pair-correlation function as in Ref. 27. This method of determining $g(\mathbf{x},\tau)$ is considerably faster than the usual direct calculation (from the real-space configuration) due to the speed and availability of fast Fourier transform routines.[37]

A. Qualitative picture

To illustrate the phenomena, run E was chosen ($\epsilon = 10^{-3}$) as a typical example. Figures 1(a)–(d) demonstrate the order parameter morphology at four different times. In Figs. 1(a) and 1(b) small inhomogeneities develop which grow in height but not in size. Gradually, domain walls form between the competing phases as is demonstrated in Fig. 1(c). Figure 1(d) shows a late-stage configuration which is dominated by interfacial dynamics (a detailed analysis of the late stages is discussed in a previous paper[27]).

In Fig. 2, the one-point distribution function $\rho_1(\psi)$ is plotted for various times for run E. Initially $\rho_1(\psi)$ has a single peak which broadens in time and gradually develops into a bimodal distribution. At this stage the bimo-

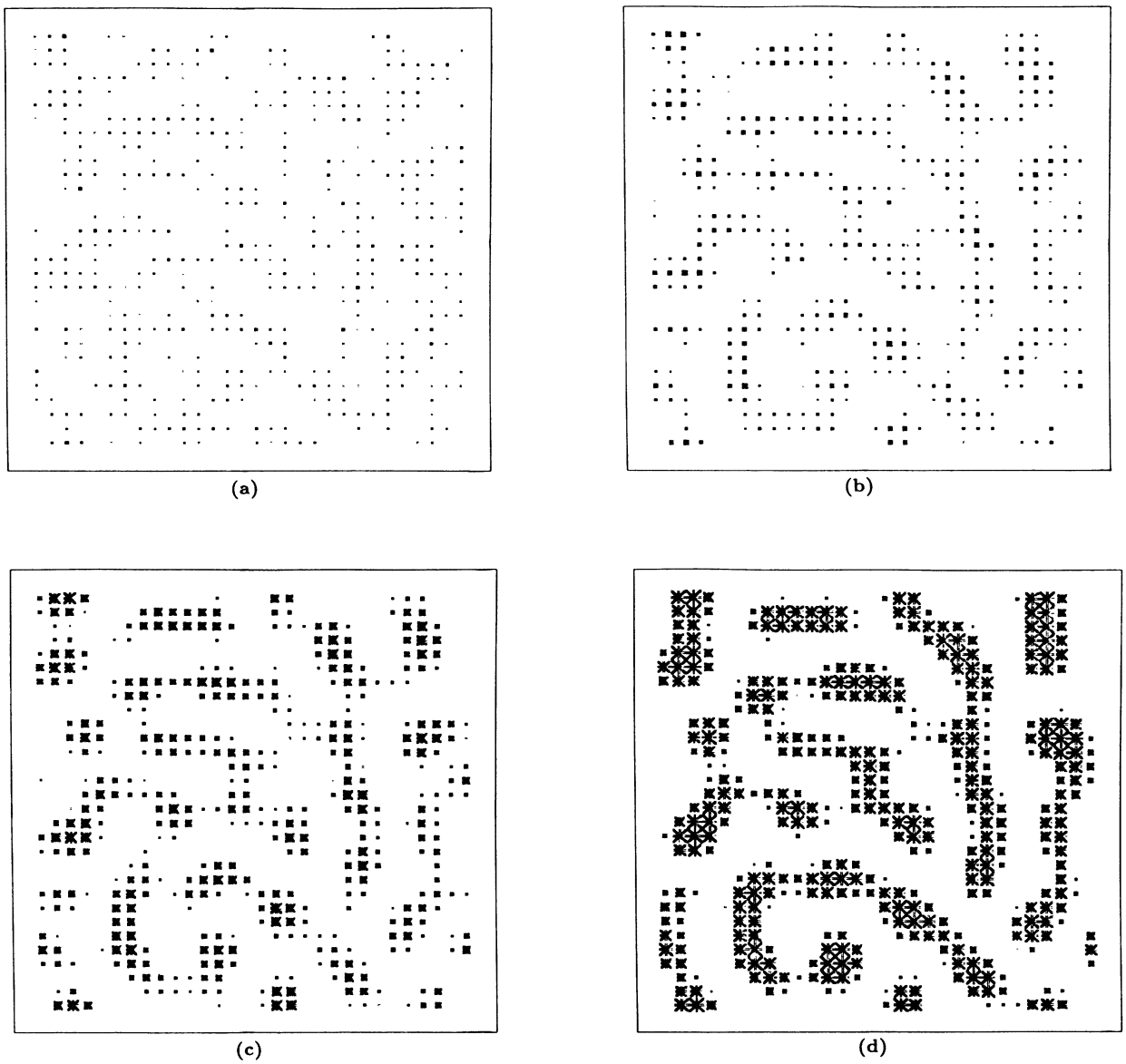

FIG. 1. Time evolution of the order-parameter field during phase separation in run E. The size of the symbol is proportional to the magnitude of ψ. (a), (b), (c), and (d) correspond to $\tau = 6$, 18, 30, and 48.

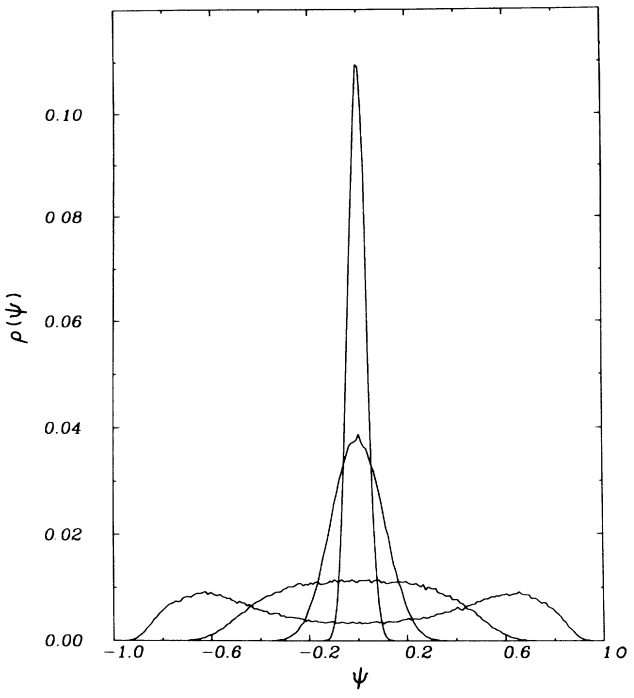

FIG. 2. Time evolution of the one-point distribution function $\rho_1(\psi)$ for run E. The lines correspond to $\tau=6$, 18, 30, and 48.

dal peaks are asymmetric about their peak position and cannot be described by the double Gaussian approximation used in NLT II (LBM).

In Figs. 3(a) and 3(b), $S(k,\tau)$ is shown at several different times for run E. Figure 3(a) shows that the peak of $S(k,\tau)$ remains fixed for the early stages. Figure 3(b) illustrates the effect of domain-wall formation and coarsening. This is exhibited by the motion of the peak inwards and the crossing of the tails of the structure factor with time.

B. Effect of ϵ and ϵ_I

To understand the effect of ϵ on domain growth, $R(\tau)$ was plotted versus $\tau^{1/3}$ for six different ϵ in Fig. 4. When comparing these curves one must remember that the initial state and noise strength are both proportional to ϵ and thus the two effects are coupled. As ϵ is increased the system begins to deviate from the linear prediction at increasingly earlier times and thus ϵ can be correlated with the effective strength of the nonlinearity. Figure 5 is a plot of $\ln[S(k_{\max},\tau)/\epsilon]$ versus τ for the six ϵ considered. Clearly the nonlinearity quickly causes the growth to deviate from exponential behavior. Together Figs. 4 and 5 indicate that the early stage development is dependent on ϵ.

To illustrate the effects of the initial conditions consider Figs. 6 and 7. The only difference between these runs and those depicted in Figs. 4 and 5 is in the initial conditions (see Table II). When ϵ_I is much greater than ϵ_N the initial state is very important. When ϵ_I is much smaller than ϵ_N, the effect of the initial state is less important. These figures show that the initial state can change the behavior of the system by inducing nonlinear effects at different times.

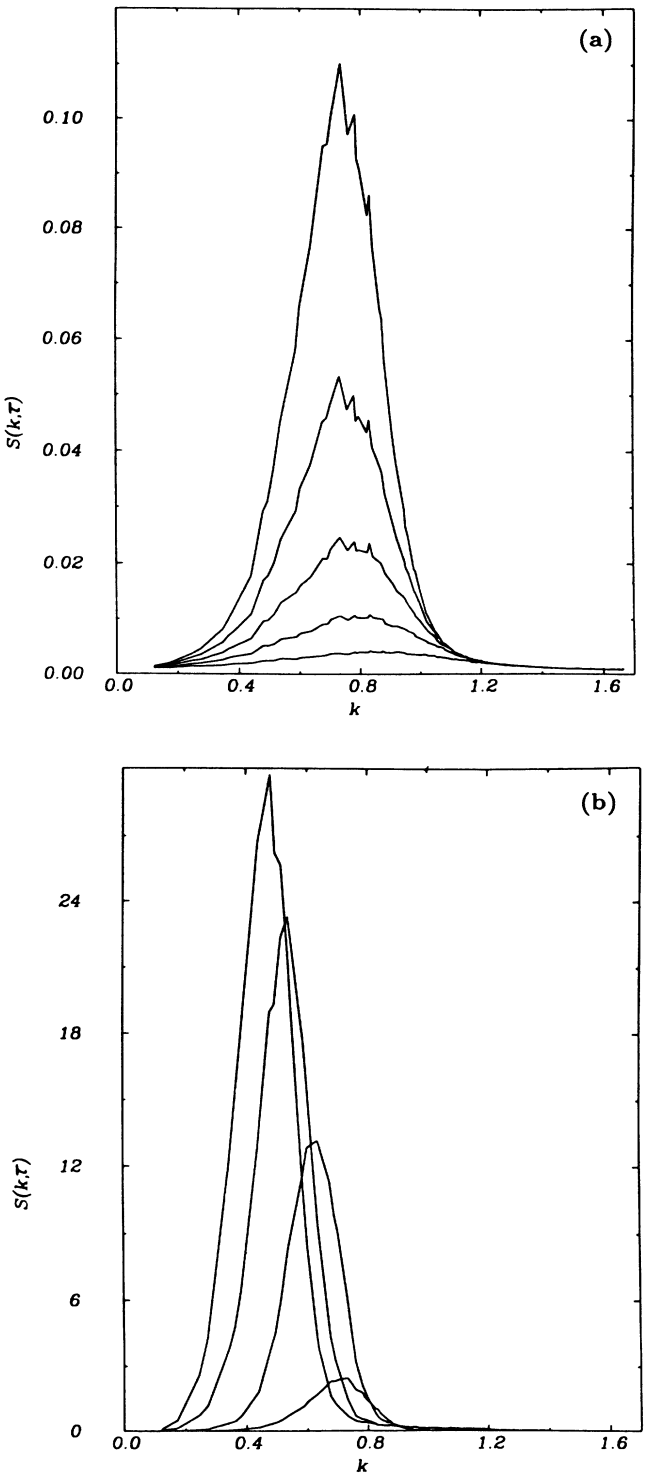

FIG. 3. Time dependence of $S(k,\tau)$ in run E. The lines in (a) from bottom to top correspond to $\tau=3$, 6, 9, 12, and 15. In (b) the lines correspond to $\tau=30$, 60, 120, and 180.

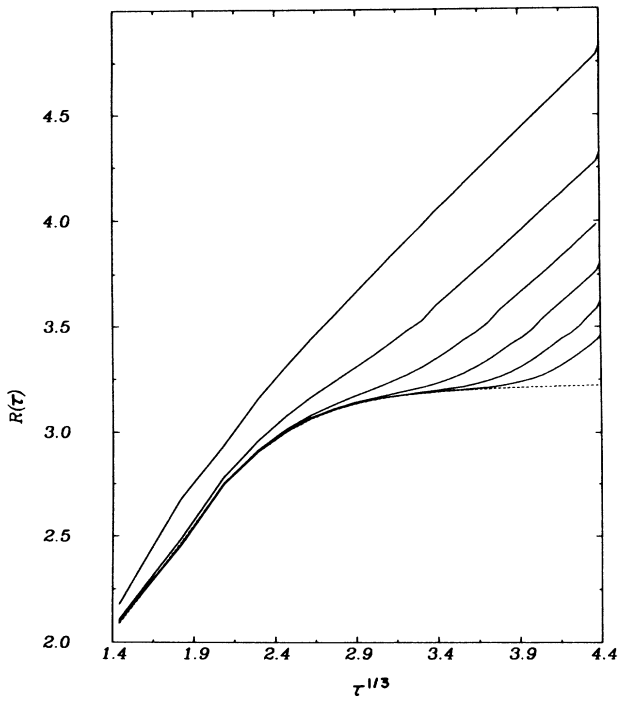

FIG. 4. The time dependence of the average domain size $R(\tau)$. From top to bottom the solid lines correspond to $\epsilon(=\epsilon_N=\epsilon_I)=10^{-1}$, 10^{-2}, 10^{-3}, 10^{-4}, 10^{-5}, and 10^{-6}. The dotted line is the LT I prediction.

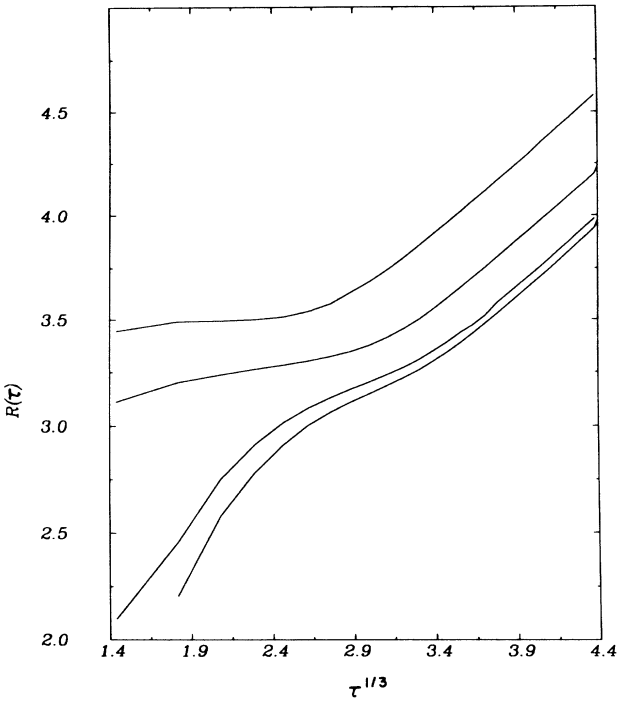

FIG. 6. The time dependence of $R(\tau)$ for $\epsilon_N=10^{-3}$ as a function of initial condition. From top to bottom the lines are $\epsilon_I=10^{-1}$, 10^{-2}, 10^{-3}, and 10^{-4}.

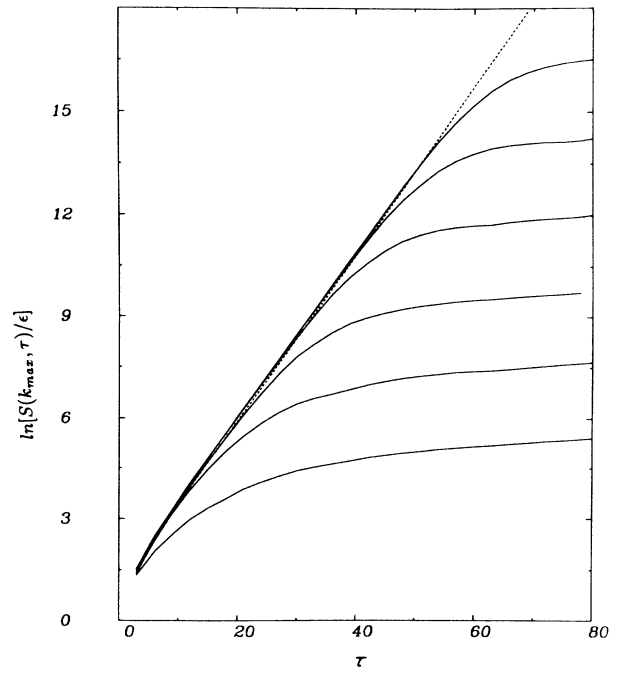

FIG. 5. The time dependence of the peak height of $S(k,\tau)$. From bottom to top the solid lines correspond to $\epsilon(=\epsilon_N=\epsilon_I)=10^{-1}$, 10^{-2}, 10^{-3}, 10^{-4}, 10^{-5}, and 10^{-6}. The dotted line is the LT I prediction.

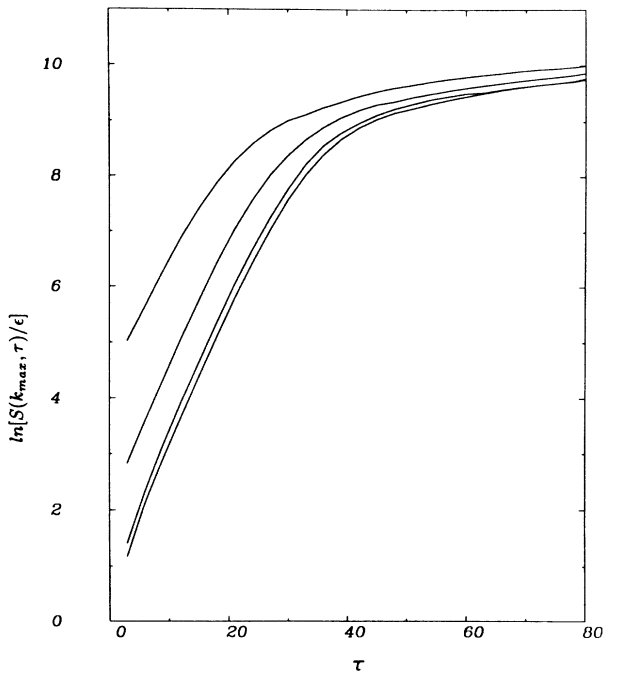

FIG. 7. The time dependence of the peak height of $S(k,\tau)$ for $\epsilon_N=10^{-3}$ as a function of initial condition. From bottom to top the lines are $\epsilon_I=10^{-1}$, 10^{-2}, 10^{-3}, and 10^{-4}.

C. Comparison of theory and simulation

Figures 8(a) and 8(b) directly compare the theoretical structure factors with the simulation results. The trends in these figures are representative of all the simulations performed. In the cases studied (i.e., the runs in Tables I and II), the NLT II (LBM) approximation is always the best, followed in order by NLT I (Gaussian), LT II, and finally LT I. Figure 9 is a plot of $R(\tau)$ versus $\tau^{1/3}$ for run E and various theories, while Fig. 10 provides a similar comparison of the peak height of $S(k,\tau)$. In Figs. 11 and 12 the theoretical predictions for $R(\tau)$ and $S_{\max}(\tau)$ are plotted and compared with run L. These figures show how the theories fare when $\epsilon_I \neq \epsilon_N$. Once again the NLT II (LBM) theory is the best followed by NLT I (Gaussian), LT II, and LT I. In all the simulations performed NLT II (LBM) breaks down in the tail portion much faster than at the peak $S(k,\tau)$. Typically the NLT II (LBM) structure factor becomes much too thin at late times.

A quantitative measure of the difference between the simulation and theories is the standard deviation (σ). In this work σ is defined as,

$$\sigma(\tau)=\left[\frac{\sum_{k,l}[S^s(k,l,\tau)-S^t(k,l,\tau)]^2}{\sum_{k,l}[S^s(k,l,\tau)]^2}\right]^{1/2} . \tag{3.2}$$

$S^t(k,l,\tau)$ is one of the four theoretical predictions and $S^s(k,l,\tau)$ is the simulated structure factor. In equilibrium $\sigma_{eq}=0.035$.

It should be noted that this definition heavily weights the peak of $S(k,\tau)$ relative to the tail since the peak is typically orders of magnitude larger than the tail. $\sigma(\tau,\epsilon)$ is plotted versus τ for all the early time theories in Fig. 13. The time of validity ($\tau_{\max}$) can be easily determined by examining this figure. It is interesting to consider the

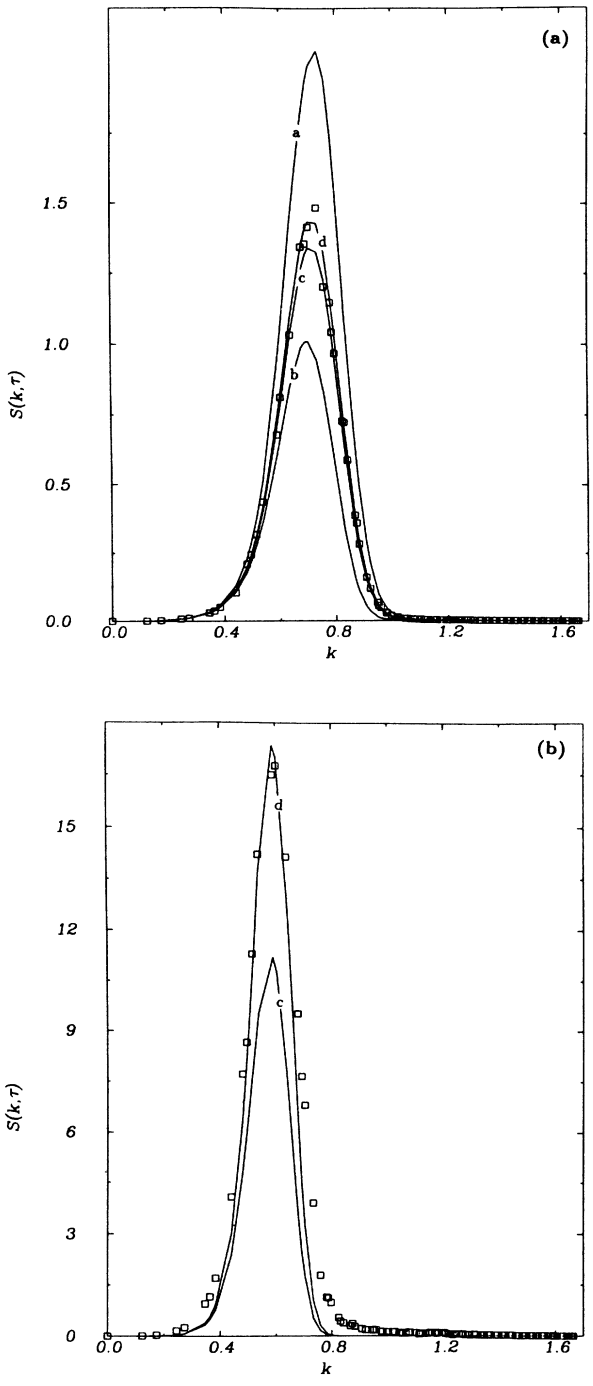

FIG. 8. Comparison of theoretical and simulated structure factor for run E. (a) and (b) correspond to $\tau=27$ and 78, respectively. In both figures line a is LT I, b is LT II, c is NLT I, and d is NLT II. The squares are the numerical simulation. In (b) the LT I and LT II are not included as they are mostly off scale.

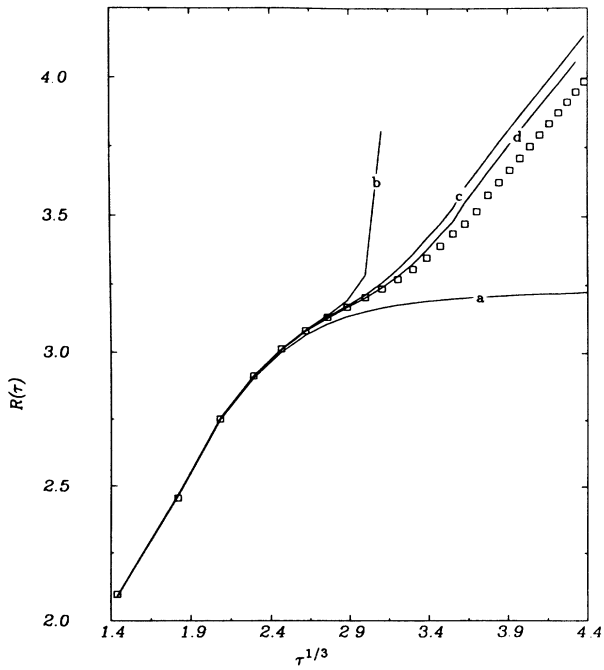

FIG. 9. Comparison of $R(\tau)$ from the numerical simulation with those from the theoretical predictions for run E. The line types and symbol are defined in Fig. 8.

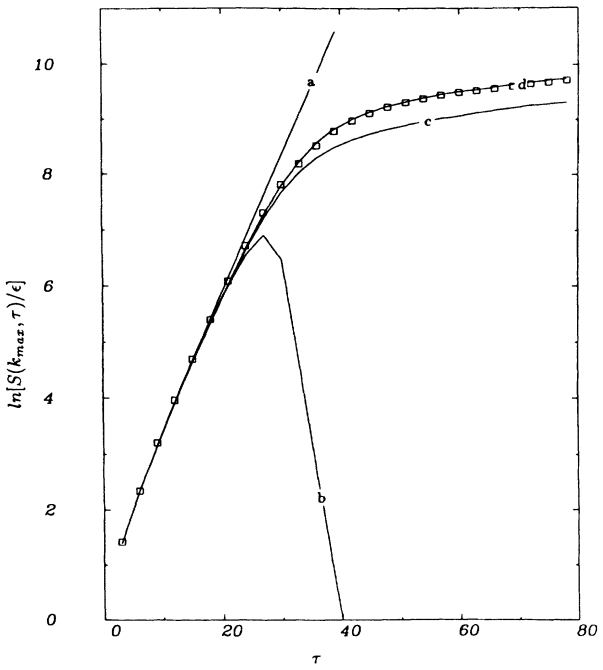

FIG. 10. Comparison of the maximum of $S(k,\tau)$ from the numerical simulation with those from the theoretical predictions for run E. The line types and symbol are defined in Fig. 8.

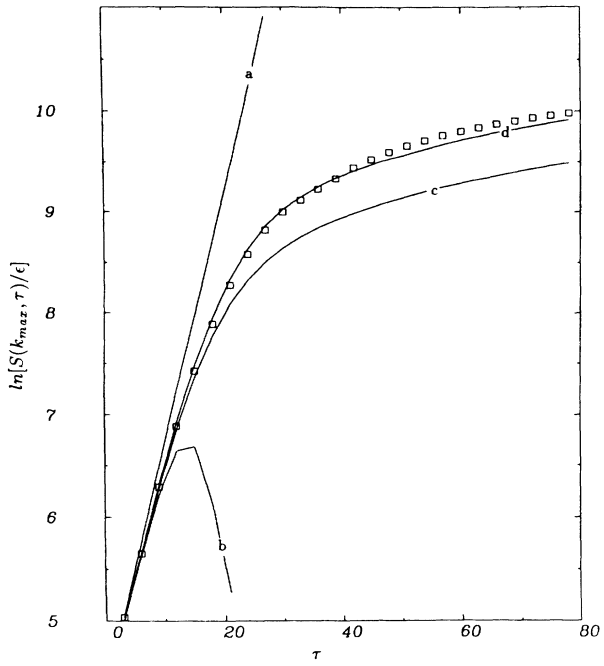

FIG. 12. Comparison of the maximum of $S(k,\tau)$ from the numerical simulation with those from the theoretical predictions for run L. The line types and symbol are defined in Fig. 8.

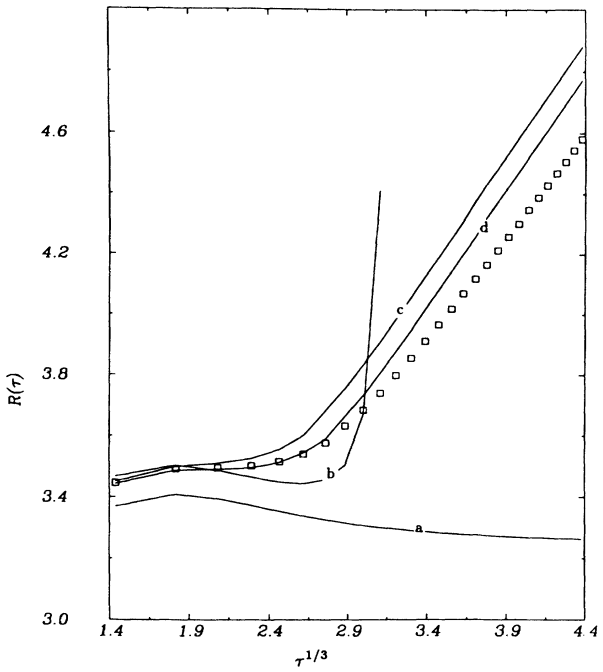

FIG. 11. Comparison of $R(\tau)$ from the numerical simulation with those from the theoretical predictions for run L. The line types and symbol are defined in Fig. 8.

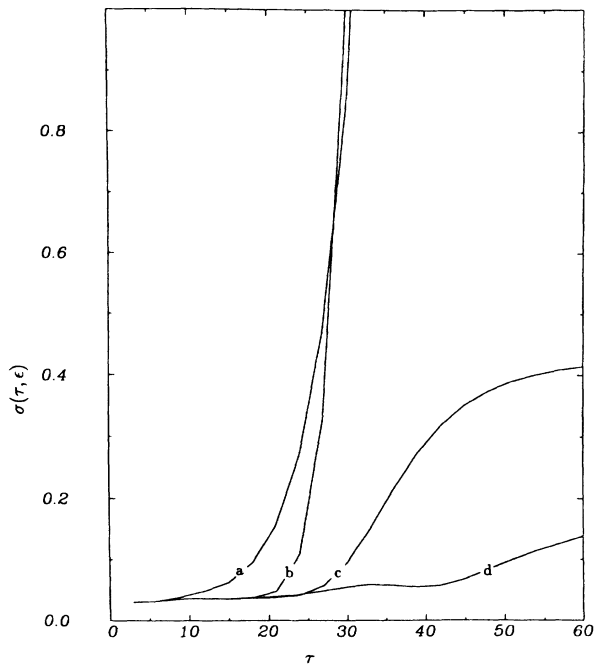

FIG. 13. The time dependence of the standard deviation between simulation and theory. The line types are defined in Fig. 8.

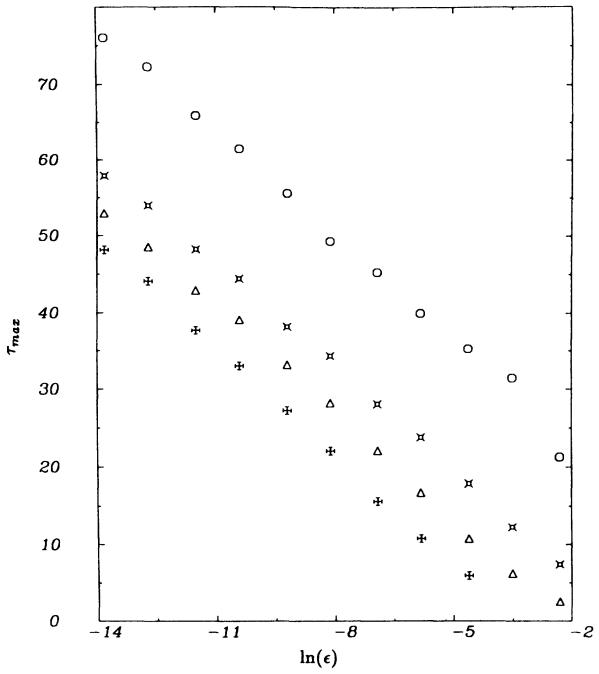

FIG. 14. The dependence of τ_{max} as a function of $\ln(\epsilon)$. The circle, star, triangle, and cross symbols correspond to NLT II, NLT I, LT II, and LT I, respectively.

way in which the theories deviate from the exact solution (i.e., the simulation). LT always break down very quickly in an exponential fashion. This is not surprising because each order term in the expansion grows exponentially whereas the exact solution grows akin to a power law. In contrast, NLT diverge from the simulation in a slower manner since they also grow in a power-law fashion (albeit the wrong power law).

To test Binder's hypothesis that the time of validity of LT I is proportional to the logarithm of ϵ, the quantity τ_{max} has to be defined. If τ_{max} is defined such that when $\sigma(\tau_{max})=x$, then $\tau_{max}(x)=A\ln(\epsilon)+B$. Varying x only has effect on B and not A. τ_{max} for all theories is plotted in Fig. 14 using $x=2\sigma_{eq}$. The values of A and B are given in Table III. It should be noted that when ϵ is large (i.e., $\epsilon>0.01$) LT I immediately diverges from the simulation and thus a value of τ_{max} cannot be obtained. The results shown in Table III indicate that A is the same for all theories but B changes in accordance with individual theories, such that B [NLT II (LBM)] $>B$[NLT I (Gaussian)] $>B$(LT II) $>B$(LT I).

TABLE III. Value of the slope and intercept of τ_{max} versus $\ln(\epsilon)$ graphs, for NLT II, NLT I, LT II, and LT I.

Theory	Slope[a]	Intercept[a]
LT I	-4.6 ± 0.1	-15 ± 1
LT II	-4.5 ± 0.1	-9 ± 1
NLT I (Gaussian)	-4.4 ± 0.1	-3 ± 1
NLT II (LBM)	-4.6 ± 0.1	$+13\pm1$

[a]The slope (A) and intercept (B) are defined such that $\tau_{max}=A\ln(\epsilon)+B$.

IV. DISCUSSION AND SUMMARY

A. Qualitative picture

A comparison of Figs. 1 and 3 indicate that the main features of the phase separation process are adequately described by $S(k,\tau)$. At early times $S(k,\tau)$ increases exponentially for small k's as small inhomogeneities begin to develop. This growth slows down gradually as ψ reaches its two-phase equilibrium values. In this time regime, small domains are formed which increase in size as interfaces begin to sharpen. The coarsening of domains moves the peak in $S(k,\tau)$ to smaller wave numbers since the peak position can roughly be correlated with the inverse of the average domain size. When interfaces are well established, the driving mechanism for further growth is the lowering of the surface curvature which amounts to lowering the surface energy. At late stages when the width of the interface is much less than the average size of the domains, $R(\tau)\sim\tau^{1/3}$.[26,27,29,34]

B. Effect of initial state

When ϵ_N is small (10^{-3}), the initial condition plays a crucial role in the early time development of $S(k,\tau)$ (see Figs. 6 and 7). This is associated with the fact that the system behaves qualitatively different in the linear (i.e., $\psi^2\gg\psi^4/2$) and nonlinear (i.e., $\psi^2\sim\psi^4/2$) regimes. For example, when the ratio ϵ_I/ϵ_N is one the system acts in a linear fashion for $\tau\lesssim12$ (see Fig. 9), but when ϵ_I/ϵ_N is 100 the system immediately enters the nonlinear regime (see Fig. 11). Clearly, the effect of the initial state depends on the relative magnitudes of ϵ_I and ϵ_N. When ϵ_I is much smaller than ϵ_N, the thermal noise quickly erases the structure of the initial state and the system is relatively insensitive to ϵ_I. However, when ϵ_I is large compared to ϵ_N the former dictates when nonlinear effects will occur.

Generally, increasing the magnitude of the fluctuations of the initial state promotes coarsening at early times, slows down exponential growth of $S(k,\tau)$ at early times, and shortens the time in which the asymptotic growth law is reached. This is especially important when the initial state is just above the critical point where ϵ_I is large. It has been clearly demonstrated that the initial state can play an important role in the early time development of $S(k,\tau)$.

C. Validity of linear theory (LT I)

When $\epsilon_I=\epsilon_N=\epsilon$, the time of validity of the linear solution is directly proportional to $\ln(\epsilon)$ which confirms Binder's[11,13] predictions. In this time regime, $f(\psi)$ is well approximated by an inverted parabola and the system grows in an exponential manner. When ϵ is large (i.e., $\epsilon>0.01$), many ψ's are already large enough that the parabolic approximation for $f(\psi)$ is invalid.

When $\epsilon_I\neq\epsilon_N$ the situation is somewhat different. In

this case linear theory will be valid only if both ϵ_I and ϵ_N are small. For example, Figs. 11 and 12 show that linear theory is never valid if $\epsilon_I = 10^{-1}$ and $\epsilon_N = 10^{-3}$ even though it is valid for $\epsilon_I = \epsilon_N = 10^{-3}$. This has interesting consequences for real experiments where the initial state depends on the quench rate.[14] In the case of two comparable experiments using different quench rates it is quite possible that one would agree with LT I and the other (i.e., the one with the slower quenched rate) would not.

It should be noted that the time independence of $R(\tau)$ is not a good criterion for assessing the validity of LT I. This is demonstrated in Figs. 9 and 11. In runs C–K, $R(\tau)$ changes with time and is in agreement with LT I (see Fig. 4). In contrast, during run L, $R(\tau)$ is relatively constant in time and linear theory is not valid (see Fig. 11). This emphasizes that care must be taken to determine when LT I is working. In an experiment where ϵ_I and ϵ_N [or $S(k,\tau=0)$] are difficult to resolve, it would be erroneous to use a time independent $R(\tau)$ as an indicator of linearity.

One final note concerning the comparison of linear theory with experiment is worth discussing. The finite time needed to measure $S(k,\tau)$ should be taken into account in an experiment. If an experimental structure factor is measured from $\tau=a$ to $\tau=b$ then it should be compared with

$$\frac{1}{b-a}\int_a^b S_1(k,\tau')d\tau'$$

and not simply $S_1(k,\tau)$. This correction assumes particular importance during early times when $(b-a)\sim\tau$. This problem is irrelevant in the case of a simulation because $S(k,\tau)$ can be measured instantaneously.

D. Comparison of theory and simulation

As expected, the inclusion of $S_3(k,\tau)$ in Eq. (2.14) provides an improvement over the linear theory. One interesting feature is that the slope of $\tau_{\max}$ versus $\ln(\epsilon)$ is virtually identical for both LT I and LT II. It is likely that the linear expansion [Eq. (2.14)] to order ϵ^j (for all j) will always break down in the same fashion (i.e., the slope of $\tau_{\max}$ versus $\ln(\epsilon)$ is constant for all j). This is due to the fact that the expansion parameter is of the form $\epsilon e^{w\tau}$.

The region of validity of the nonlinear theories also appears to be logarithmically related to ϵ. In fact, the slope of $\tau_{\max}$ versus $\ln(\epsilon)$ is very close to that of the LT theories, the only difference being in the intercept which is greater for the nonlinear theories. The improvement NLT II (LBM) provides over NLT I (Gaussian) is mainly in the prediction of $S_{\max}(\tau)$. Unfortunately, NLT II (LBM) fails to properly account for the tail portion of $S(k,\tau)$. In fact, as NLT II (LBM) $S(k,\tau)$ deviates from the "exact" solution it becomes much too narrow. A similar discrepancy is apparent in the comparison provided in Ref. 7 of LBM theory with a three-dimensional Monte Carlo study. This deficiency is linked to the lack of direct coupling of Fourier modes. In both NLT theories the coupling (due to the nonlinear term) of the maximum Fourier component of the order parameter to the higher-order Fourier modes is not adequately described by the mean-field approximation.

The width of the structure factor is affected by the interfacial structure. For example, a system of well-defined interfaces will produce a much broader structure factor than a system containing very diffuse interfaces. The narrowness of the NLT II (LBM) $S(k,\tau)$ is therefore consistent with a system of broad interfaces.

In contrast, the linear expansion does have the necessary ingredients to describe sharp interfaces. However, the difficulty here is that all terms in the expansion must be taken into account to properly describe well-defined interfaces. Although the second term in the expansion will help sharpen the interfaces, it quickly becomes inadequate as domain walls between competing phases develop.

Another interesting difference between the theories is the manner in which they slow down the initial exponential growth. In the perturbative expansion each term grows exponentially faster than the previous term so that the solution will always diverge. Since the series alternates the solution will diverge to $\pm\infty$ depending on whether the number of terms included is even or odd. As a result theories based on a linear propagator will always break down in an exponential fashion if only a finite number of terms are included. In contrast the NLT theories grow as a power law.

E. Summary

The validity of the current early time theories of spinodal decomposition have been quantitatively assessed. A linear regime has been clearly identified which is marked by the exponential growth of the structure factor. Transition from this linear domain to the asymptotic scaling regime is a complex phenomenon. A very intricate coupling of all modes is needed to properly describe the formation of sharp domain walls. Unfortunately, use of a "mean-field" coupling in the nonlinear type theories is insufficient to properly describe these late stage effects. Although the linear expansion correctly incorporates this subtle coupling it is difficult to implement due to the increasing complexity of each successive term in the expansion. At present a first principles understanding of domain-wall formation does not exist.

In summary, the numerical simulation used has provided detailed insight into the inadequacies of the current early time theories and the effects of the initial state on the time development of $S(k,\tau)$.

APPENDIX A

In Eq. (2.14) $\epsilon=\epsilon_I=\epsilon_N$. In the general case, when ϵ_I and ϵ_N are different, the second term in expansion [i.e., $\epsilon^2 S_3(k,n)$] will be denoted $\hat{S}_3(k,n)$. $\hat{S}_3(k,n)$ is then

$$\hat{S}_3(k,n)=\frac{3a^{2n-1}(k)[\Gamma(k)\Delta\tau]^2}{\epsilon^2}\times\left[\frac{\epsilon_I^2 H(1)+\epsilon_I\epsilon_N H(2)}{1-d^2(k)}+\frac{\epsilon_I\epsilon_N H(3)+\epsilon_N^2 H(4)}{1-a^2(k)}\right], \tag{A1}$$

where

$$H(1)=(\Delta x N)^{-2}\sum_{\mathbf{k}'}\left[\frac{-\Delta\tau\Gamma(k')}{1-d^2(k')}\right]\left[\frac{1-a^{2n}(k')}{1-a^2(k')}\right],$$

$$H(2)=(\Delta x N)^{-2}\sum_{\mathbf{k}'}\left[\frac{-\Delta\tau\Gamma(k')}{1-a^2(k')}\right]\left[n-\frac{1-a^{2n}(k')}{1-a^2(k')}\right],$$

$$H(3)=\frac{a(k)}{(\Delta x N)^2}\sum_{\mathbf{k}'}\left[\frac{-\Delta\tau\Gamma(k')}{1-d^2(k')}\right]\times\left[\frac{[a(k')/a(k)]^{2n}-1}{a^2(k')-a^2(k)}\right]-H(1),$$

$$H(4)=\frac{-a(k)}{(\Delta x N)^2}\sum_{\mathbf{k}'}\left[\frac{-\Delta\tau\Gamma(k')}{1-a^2(k')}\right]\times\left[\frac{[a(k')/a(k)]^{2n}-1}{a^2(k')-a^2(k)}+\frac{1-a^{-2n}(k)}{1-a^2(k)}\right]-H(2).$$

$H(1)$ is due strictly to the initial state, $H(2)$ and $H(3)$ are due to combinations of the initial state and the thermal fluctuations, and $H(4)$ is only influenced by the thermal fluctuations.

APPENDIX B

To minimize the effect of roundoff error,[7] an equation of motion for the cumulant,

$$\langle\psi^4(n)\rangle_c\equiv\langle\psi^4(n)\rangle-3\langle\psi^2(n)\rangle^2$$

will be described instead of the EOM for $\langle\psi^4(n)\rangle$ itself. To facilitate the following derivation it is useful to write Eq. (2.9) in the following notation:

$$\psi(\mathbf{r},n+1)=\sum_{\mathbf{r}'}[\gamma_{\mathbf{r},\mathbf{r}'}\psi(\mathbf{r},n)+\beta_{\mathbf{r},\mathbf{r}'}\psi^3(\mathbf{r},n)], \tag{B1}$$

where

$$\gamma_{\mathbf{r},\mathbf{r}'}=\delta_{\mathbf{r},\mathbf{r}'}-\frac{\Delta\tau}{2}\left[\Gamma_{\mathbf{r},\mathbf{r}'}+\sum_{\mathbf{r}''}\Gamma_{\mathbf{r},\mathbf{r}'}\Gamma_{\mathbf{r}'',\mathbf{r}'}\right],$$

$$\beta_{\mathbf{r},\mathbf{r}'}=\frac{\Delta\tau}{2}\Gamma_{\mathbf{r},\mathbf{r}'},$$

$$\Gamma_{\mathbf{r},\mathbf{r}'}=(\Delta x)^{-2}(\delta_{i,i'}\delta_{j,j'-1}+\delta_{i,i'}\delta_{j,j'+1}+\delta_{i,i'-1}\delta_{j,j'}+\delta_{i,i'+1}\delta_{j,j'}-4\delta_{i,i'}\delta_{j,j'}),$$

$$\mathbf{r}=\Delta x(i\hat{\mathbf{x}}+j\hat{\mathbf{y}}).$$

The noise term cancels out in the cumulant EOM for the fourth moment, and thus is not included in Eq. (B1). In this notation the EOM for $\langle\psi^4(n)\rangle_c$, is

$$\begin{aligned}\langle\psi^4(n+1)\rangle_c=&\{\langle[\gamma\psi(n+1)]^4\rangle-3\langle[\gamma\psi(n+1)]^2\rangle^2\}+4[\langle(\gamma\psi)^3(\beta\psi^3)\rangle-3\langle(\gamma\psi)(\beta\psi^3)\rangle\langle(\gamma\psi)^2\rangle]\\&+6[\langle(\gamma\psi)^2(\beta\psi^3)^2\rangle-2\langle(\gamma\psi)(\beta\psi^3)\rangle-\langle(\gamma\psi)^2\rangle\langle(\beta\psi^3)^2\rangle]\\&+4[\langle(\gamma\psi)(\beta\psi^3)^3\rangle-3\langle(\gamma\psi)(\beta\psi^3)\rangle\langle(\beta\psi^3)^2\rangle]+[\langle(\beta\psi^3)^4\rangle-3\langle(\beta\psi^3)^2\rangle^2],\end{aligned} \tag{B2}$$

where

$$\gamma\psi\equiv\sum_{\mathbf{r}'}\gamma_{\mathbf{r},\mathbf{r}'}\psi(\mathbf{r},n),$$

$$\beta\psi^3\equiv\sum_{\mathbf{r}'}\beta_{\mathbf{r},\mathbf{r}'}\psi^3(\mathbf{r},n).$$

The first term ($T1$) on the right-hand side of Eq. (B2), i.e.,

$$T1\equiv\sum_{\mathbf{r}_1,\mathbf{r}_2,\mathbf{r}_3,\mathbf{r}_4}\gamma_{\mathbf{r},\mathbf{r}_1}\gamma_{\mathbf{r},\mathbf{r}_2}\gamma_{\mathbf{r},\mathbf{r}_3}\gamma_{\mathbf{r},\mathbf{r}_4}(\langle\psi_{\mathbf{r}_1}\psi_{\mathbf{r}_2}\psi_{\mathbf{r}_3}\psi_{\mathbf{r}_4}\rangle-\langle\psi_{\mathbf{r}_1}\psi_{\mathbf{r}_2}\rangle\langle\psi_{\mathbf{r}_3}\psi_{\mathbf{r}_4}\rangle)$$

can be split into four pieces in the following manner,

$$\begin{aligned}T1=&\sum_{\mathbf{r}_1}\gamma_{\mathbf{r},\mathbf{r}_1}^4(\langle\psi^4\rangle-3\langle\psi^2\rangle^2)+4\sum_{\mathbf{r}_1}\sum_{\mathbf{r}_2\neq\mathbf{r}_1}\gamma_{\mathbf{r},\mathbf{r}_1}^3\gamma_{\mathbf{r},\mathbf{r}_2}(\langle\psi_{\mathbf{r}_1}^3\psi_{\mathbf{r}_2}\rangle-3\langle\psi^2\rangle\langle\psi_{\mathbf{r}_1}\psi_{\mathbf{r}_2}\rangle)\\&+3\sum_{\mathbf{r}_1}\sum_{\mathbf{r}_2\neq\mathbf{r}_1}\gamma_{\mathbf{r},\mathbf{r}_1}^2\gamma_{\mathbf{r},\mathbf{r}_2}^2(\langle\psi_{\mathbf{r}_1}^2\psi_{\mathbf{r}_2}^2\rangle-2\langle\psi^2\rangle^2-\langle\psi_{\mathbf{r}_1}\psi_{\mathbf{r}_2}\rangle^2)\\&+\sum_{\mathbf{r}_1,\mathbf{r}_2,\mathbf{r}_3,\mathbf{r}_4}^{*}\gamma_{\mathbf{r},\mathbf{r}_1}\gamma_{\mathbf{r},\mathbf{r}_2}\gamma_{\mathbf{r},\mathbf{r}_3}\gamma_{\mathbf{r},\mathbf{r}_4}(\langle\psi_{\mathbf{r}_1}\psi_{\mathbf{r}_2}\psi_{\mathbf{r}_3}\psi_{\mathbf{r}_4}\rangle-\langle\psi_{\mathbf{r}_1}\psi_{\mathbf{r}_2}\rangle\langle\psi_{\mathbf{r}_3}\psi_{\mathbf{r}_4}\rangle,\end{aligned}$$

where $\sum^*$ is a sum over all $\mathbf{r}_1$, $\mathbf{r}_2$, $\mathbf{r}_3$, and $\mathbf{r}_4$ except for the following situations:

(i) $(\mathbf{r}_1=\mathbf{r}_2=\mathbf{r}_3=\mathbf{r}_4)$,

(ii) $(\mathbf{r}_1=\mathbf{r}_2=\mathbf{r}_3;\mathbf{r}_4)$, $(\mathbf{r}_1=\mathbf{r}_2=\mathbf{r}_4;\mathbf{r}_3)$, $(\mathbf{r}_1=\mathbf{r}_3=\mathbf{r}_4;\mathbf{r}_2)$, $(\mathbf{r}_2=\mathbf{r}_3=\mathbf{r}_4;\mathbf{r}_1)$,

(iii) $(\mathbf{r}_1=\mathbf{r}_2;\mathbf{r}_3=\mathbf{r}_4)$, $(\mathbf{r}_1=\mathbf{r}_3;\mathbf{r}_2=\mathbf{r}_4)$, $(\mathbf{r}_1=\mathbf{r}_4;\mathbf{r}_2=\mathbf{r}_3)$.

The first three terms in $T1$ contain only one- and two-point correlations and can be determined by Eqs. (2.17) and (2.19). The last term has three-point and higher correlations. These higher-order correlations should be considerably smaller than the one- and two-point correlations and thus will be neglected. This term is also small because it is $\sim(\Delta\tau)^2$ and would not appear in the continuous case. With these approximations $T1$ becomes

$$T1=\langle\psi^4(n)\rangle_c\left[4\sum_{\mathbf{r}_1,\mathbf{r}_2}\gamma^3_{\mathbf{r},\mathbf{r}_1}\gamma_{\mathbf{r},\mathbf{r}_2}\frac{g(\mathbf{r}_1-\mathbf{r}_2,n)}{\langle\psi^2(n)\rangle}-3\sum_{\mathbf{r}_1}\gamma^4_{\mathbf{r},\mathbf{r}_1}\right]-6\left[\sum_{\mathbf{r}_1,\mathbf{r}_2}\gamma^2_{\mathbf{r},\mathbf{r}_1}\gamma^2_{\mathbf{r},\mathbf{r}_2}g^2(\mathbf{r}_1-\mathbf{r}_2,n)-\langle\psi^2(n)\rangle^2\sum_{\mathbf{r}_1}\gamma^4_{\mathbf{r},\mathbf{r}_1}\right].$$

In a similar fashion all terms on the right-hand side of Eq. (B2) can be determined. The final result is

$$\begin{aligned}\langle\psi^4(n+1)\rangle_c=&\langle\psi^4(n)\rangle_c[4(S^{(1)}_{\gamma,\gamma,\gamma,\gamma}+RS^{(1)}_{\gamma,\gamma,\gamma,\beta})-3S^{(0)}_{\gamma,\gamma,\gamma,\gamma}-4RS^{(0)}_{\gamma,\gamma,\gamma,\beta}]\\&+\langle\psi^6(n)\rangle^*[3(S^{(1)}_{\gamma,\gamma,\beta,\gamma}+RS^{(1)}_{\gamma,\gamma,\beta,\beta})-2S^{(0)}_{\gamma,\gamma,\gamma,\beta}-3RS^{(0)}_{\gamma,\gamma,\beta,\beta}]\\&+\langle\psi^8(n)\rangle^*[2(S^{(1)}_{\gamma,\beta,\beta,\gamma}+RS^{(1)}_{\gamma,\beta,\beta,\beta})-1S^{(0)}_{\gamma,\gamma,\beta,\beta}-2RS^{(0)}_{\gamma,\beta,\beta,\beta}]\\&+\langle\psi^{10}(n)\rangle^*[1(S^{(1)}_{\beta,\beta,\beta,\gamma}+RS^{(1)}_{\beta,\beta,\beta,\beta})-RS^{(0)}_{\beta,\beta,\beta,\beta}]+\langle\psi^{12}(n)\rangle^*[+1S^{(0)}_{\beta,\beta,\beta,\beta}]\\&-6[S^{(2)}_{\gamma,\gamma,\gamma,\gamma}+4RS^{(2)}_{\gamma,\gamma,\gamma,\beta}+2R^2(S^{(2)}_{\gamma,\gamma,\beta,\beta}+S^{(2)}_{\gamma,\beta,\gamma,\beta})+4R^3S^{(2)}_{\gamma,\beta,\beta,\beta}+R^4S^{(2)}_{\beta,\beta,\beta,\beta}]\\&+6[S^{(0)}_{\gamma,\gamma,\gamma,\gamma}+4RS^{(0)}_{\gamma,\gamma,\gamma,\beta}+6R^2S^{(0)}_{\gamma,\gamma,\beta,\beta}+4R^3S^{(0)}_{\gamma,\beta,\beta,\beta}+R^4S^{(0)}_{\beta,\beta,\beta,\beta}],\end{aligned}\tag{B3}$$

where

$$R\equiv\frac{\langle\psi^4(n)\rangle}{\langle\psi^2(n)\rangle},$$

$$\langle\psi^6(n)\rangle^*\equiv\langle\psi^6(n)\rangle-3\langle\psi^2(n)\rangle\langle\psi^4(n)\rangle,$$

$$\langle\psi^8(n)\rangle^*\equiv\langle\psi^8(n)\rangle-2\langle\psi^4(n)\rangle^2-\langle\psi^2(n)\rangle\langle\psi^6(n)\rangle,$$

$$\langle\psi^{10}(n)\rangle^*\equiv\langle\psi^{10}(n)\rangle-3\langle\psi^4(n)\rangle\langle\psi^6(n)\rangle,$$

$$\langle\psi^{12}(n)\rangle^*\equiv\langle\psi^{12}(n)\rangle-3\langle\psi^6(n)\rangle^2,$$

$$S^{(0)}_{w,x,y,z}\equiv\sum_{\mathbf{r}_1}w_{\mathbf{r},\mathbf{r}_1}x_{\mathbf{r},\mathbf{r}_1}y_{\mathbf{r},\mathbf{r}_1}z_{\mathbf{r},\mathbf{r}_1},$$

$$S^{(1)}_{w,x,y,z}\equiv\sum_{\mathbf{r}_1,\mathbf{r}_2}w_{\mathbf{r},\mathbf{r}_1}x_{\mathbf{r},\mathbf{r}_1}y_{\mathbf{r},\mathbf{r}_1}z_{\mathbf{r},\mathbf{r}_2}\frac{g(\mathbf{r}_1-\mathbf{r}_2,n)}{\langle\psi^2(n)\rangle},$$

$$S^{(2)}_{w,x,y,z}=\sum_{\mathbf{r}_1,\mathbf{r}_2}w_{\mathbf{r},\mathbf{r}_1}x_{\mathbf{r},\mathbf{r}_1}y_{\mathbf{r},\mathbf{r}_2}z_{\mathbf{r},\mathbf{r}_2}g^2(\mathbf{r}_1-\mathbf{r}_2,n),$$

and w, x, y, and z are γ or β. It should be noted that it is much more efficient to evaluate the functions $S^{(i)}_{w,x,y,z}(n)$ (for $i=1$ and 2) in k space due to the speed of packaged Fourier transform routines.

The two parameters σ and b that completely specify $\rho_2(\psi_1,\psi_2)$ are determined by the following relationships,

$$\sigma=\langle\psi^2\rangle-b^2,$$

and

$$b^4=-\langle\psi^4\rangle_c/2.$$

All the higher-order moments can be described in terms of σ and b through Eq. (2.19).

ACKNOWLEDGMENTS

We would like to thank Martin Grant, Gian-Luca Oppo, and Ray Kapral for stimulating discussions. We gratefully acknowledge IBM-Canada for use of an IBM-3081. This work is also supported by the Natural Sciences and Engineering Research Council of Canada.

[1] J. D. Gunton, M. San Miguel, and P. Sahni, in *Phase Transitions and Critical Phenomena*, edited by C. Domb and J. L. Lebowitz (Academic, London, 1983), Vol. 8, p. 267, and references therein.
[2] J. W. Cahn and J. E. Hilliard, J. Chem. Phys. **28**, 258 (1958).
[3] J. W. Cahn, Acta. Metall. **9**, 795 (1961).
[4] H. E. Cook, J. Chem. Solids **30**, 2427 (1969).
[5] H. E. Cook, Acta. Metall. **18**, 297 (1970).
[6] J. S. Langer, Ann. Phys. **65**, 53 (1971).
[7] J. S Langer, M. Bar-on, and H. D. Miller, Phys. Rev. A **11**, 1417 (1975).
[8] K. Binder, Phys. Rev B **15**, 4425 (1977).
[9] K. Binder, C. Billotet, and P. Mirold, Z. Phys. B **30**, 183 (1978).
[10] C. Billotet and K. Binder, Z. Phys. B **32**, 195 (1979).
[11] K. Binder, Phys. Rev. A **29**, 341 (1984).
[12] M. Grant, M. San Miguel, J. Vinals, and J. D. Gunton, Phys Rev. B **31**, 3027 (1985).
[13] K. Binder, Physica **140A**, 35 (1986).
[14] H.-O. Carmesin, D. W. Heermann, and K. Binder, Z. Phys. B **65**, 89 (1986).
[15] A. B. Bortz, M. H. Kalos, J. L. Lebowitz, and M. A. Zendejas, Phys. Rev. **10**, 535 (1974).
[16] J. L. Lebowitz, J. Marro, and M. H. Kalos, Acta. Metall. **30**, 297 (1982).
[17] J. Marro and J. L. Valles, Phys. Lett. **95A**, 443 (1983).
[18] P. Meakin, H. Metiu, R. G. Petschek, and D. J. Scalapino, J. Chem. Phys. **79**, 1948 (1983); R. G. Petschek and H. Metiu, *ibid.* **79**, 3443 (1983).

[19]S. W. Koch, R. C. Desai, and F. F. Abraham, Phys. Rev. A **27**, 2152 (1983).
[20]D. Heermann, Phys. Rev. Lett. **52**, 1126 (1984); D. Heermann, Z. Phys. B **61**, 311 (1985).
[21]R. Kapral, Phys. Rev. A **31**, 3868 (1985); G. -L. Oppo and R. Kapral, *ibid.* **33**, 4219 (1986); R. Kapral and G.-L. Oppo, Physica **23D**, 455 (1986).
[22]Y. Oono and S. Puri, Phys. Rev. Lett. **58**, 836 (1987).
[23]G. F. Mazenko and O. T. Valls, Phys. Rev. Lett. **59**, 680 (1987).
[24]J. G. Amar, F. E. Sullivan, and R. D. Mountain, Phys. Rev. B **37**, 196 (1988).
[25]A. Milchev, D. W. Heermann, and K. Binder, Acta. Metall. **36**, 377 (1988).
[26]E. T. Gawlinski, J. D. Gunton, and J. Vinals (unpublished).
[27]T. M. Rogers, K. R. Elder, and R. C. Desai, Phys. Rev. B **37**, 9638 (1988).
[28]N. C. Wong and C. M. Knobler, J. Chem. Phys. **69**, 725 (1978).
[29]Y. C. Chou and W. I. Goldburg, Phys. Rev. A **23**, 858 (1981).
[30]N. C. Wong and C. M. Knobler, Phys. Rev. A **24**, 3205 (1981).
[31]M. Furusaka, Y. Ishikawa, and M. Mera, Phys. Rev. Lett. **54**, 2611 (1985).
[32]T. Izumitani and T. Hashimoto, J. Chem. Phys. **87**, 3694 (1985).
[33]H. Tanaka and T. Nishi, Phys. Rev. Lett. **59**, 692 (1987).
[34]B. D. Gaulin, S. Spooner, and Y. Morii, Phys. Rev. Lett. **59**, 668 (1987).
[35]M. Suzuki, J. Stat. Phys. **16**, 11 (1977).
[36]K. Kawasaki, M. C. Yalabik, and J. D. Gunton, Phys. Rev. A **17**, 455 (1978).
[37]The CPU time to calculate $g(r,\tau)$ for 250 runs of a 30×30 system on a Sun 3/260 workstation with a floating point accelerator is 1450 s for a direct real-space calculation and 121 s using the Fourier transform routines.